ACS APPLIED MATERIALS & INTERFACES
Research Article
www.acsami.org

Postfabrication Annealing Effects on Insulator−Metal Transitions in VO_2 Thin-Film Devices

Servin Rathi,[†] In-yeal Lee,[†] Jin-Hyung Park,[†] Bong-Jun Kim,[‡] Hyun-Tak Kim,[‡,§] and Gil-Ho Kim*,[†]

[†]School of Electronic and Electrical Engineering and Sungkyunkwan Advanced Institute of Nanotechnology (SAINT), Sungkyunkwan University, Suwon 440-746, Korea

[‡]Metal−Insulator Transition Creative Research Center, ETRI, Daejeon 305-700, Korea

[§]School of Advanced Device Technology, Korean University of Science & Technology, Daejeon 305-700, Korea

Supporting Information

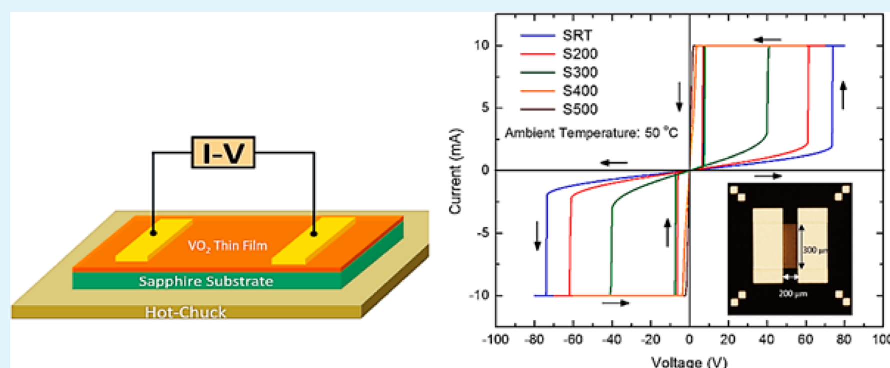

ABSTRACT: In order to investigate the metal−insulator transition characteristics of VO_2 devices annealed in reducing atmosphere after device fabrication at various temperature, electrical, chemical, and thermal characteristics are measured and analyzed. It is found that the sheet resistance and the insulator−metal transition point, induced by both voltage and thermal, decrease when the devices are annealed from 200 to 500 °C. The V $2p_{3/2}$ peak variation in X-ray photoelectron spectroscopy (XPS) characterization verifies the reduction of thin-films. A decrease of the transition temperature from voltage hysteresis measurements further endorse the reducing effects of the annealing on VO_2 thin-film.

KEYWORDS: *vanadium dioxide thin-films, annealing, metal−insulator transition, transmission line method*

1. INTRODUCTION

Dimerization and tilting of the vanadium chains leads to localization of $3d^1$ electrons, which results in the splitting of d_{11} orbital resulting in a small band gap of 0.6 eV; thus, an insulating behavior of VO_2 can be observed at room-temperature.[1,2] However, this localization of electrons can be overcome with an external stimuli such as thermal, electrical, strain, etc., which leads to an abrupt jump in the conductivity along with the lattice reorientation from monoclinic to tetragonal with vanadium atoms aligned in parallel chains.[3−5] Both Motts and Peierls transition theories based on critical electrons and phonon densities, respectively, hold valid in the case of VO_2 transitions; however, a definite mechanism is still elusive. Besides providing an excellent platform for the rich correlation study, the applications side of VO_2 also hold huge potential in sensing, switching, memristors, and smart window applications.[6−9] With a switching time of an order of picosecond and insulator−metal transition at 67 °C with a wide hysteresis, both switching and memory applications holds potential. The role of electric-field and joule-heating in electrical transition is still debatable where various studies have indicated the role of both factors in the transition.[10,11] Apart from the switching mechanism the dependency of transition point on the stoichiometry of VO_2 thin-films have also been the subject of recent studies where the stoichiometry is varied by changing the oxygen partial pressure during the film deposition.[12,13] Variation in transition temperature with oxygen partial pressure has been observed and attributed to the formation of other higher (lower) vanadium oxides including magneli phases. Besides these in situ studies, the behavior of thin-film characteristics postfabrication also needs to be studied for the variation of device characteristics as a function of ambient conditions. Here, we have performed the annealing experiment to study the variation in the transition characteristics of the thin-film. For this, both Transmission Line Method (TLM) pattern and two-terminal devices are fabricated. X-ray photoelectron spectroscopy (XPS) technique is used to investigate the stoichiometric change in the thin-films using (ESCA 2000, VG Microtech: U.K.) twin anode X-ray sources Kα (1486.6 eV)/Mg Kα (1253.6 eV) in a vacuum of 10^{-9} Torr.

Received: July 19, 2014
Accepted: October 24, 2014
Published: October 24, 2014

© 2014 American Chemical Society

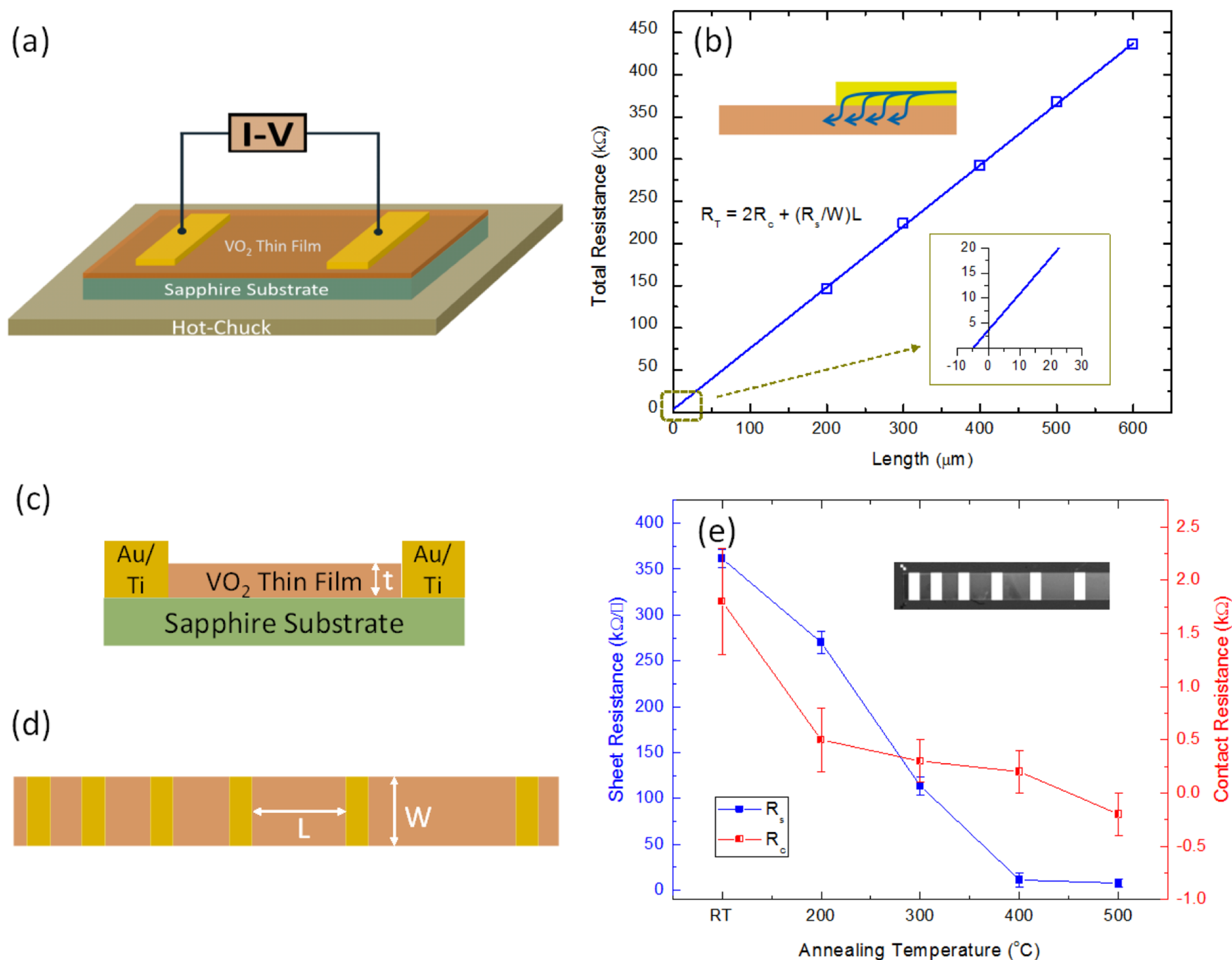

Figure 1. Schematic of VO_2 devices used for TLM and high temperatures measurement for contact, sheet resistances, and transition voltages. (a) Schematic for high-temperature measurement. (b) Total resistance vs length fitted with linear curve for TLM. The top left inset shows conduction path at the Ohmic contact while the bottom-right inset zoom-in encircled area for more clarity. (c) Cross-sectional view of the device; (d) top-view of the device for TLM. (e) Sheet resistance and contact resistance for various devices annealed at various temperature. The inset shows the fabricated device with channel width of 500 μm.

The transition characteristics are measured by $I-V$ curves at different ambient temperatures. The results obtained correlates well with the power model and simulated results based on joule-heating.

2. EXPERIMENTAL DETAILS AND CHARACTERIZATION

The VO_2 thin-films were successfully grown on α-Al_2O_3 (1012) substrates by laser ablation with a vanadium metal target in an ambient of a partially filled oxygen and argon. The KrF excimer laser (Lambda-Physik, Compex 205) with a wavelength of 248 nm was used to ablate the rotating metal target. An energy intensity of 1−2 J/cm^2 was focused on the target surface at repetition rate of 5 Hz. The distance between the target and the substrate was 5 cm. The chamber was evacuated down to the base pressure as low as 10^{-6} Torr. Argon and oxygen gases were filled by adjusting the gas-flow meter. The substrate temperature was kept at 450 °C during the deposition process. The film growth was carried out at a pressure between 50 and 200 mTorr. The partial pressure of oxygen was the most critical variable in obtaining the pure VO_2 phase, which was controlled by the working pressure containing 10% oxygen in an argon atmosphere. The deposition rate of VO_2 films was estimated to be about 0.39 A/s and thin-films of various thickness were deposited. After deposition, the substrates were slowly cooled to the room temperature under the same deposition atmosphere as that used for growth. XPS and Raman characterization of the thin-films (see Supporting Information) shows good quality deposition of thin-films. After patterning, the thin-film were etched using O_2/CF_4 gases and device fabrication is carried out using typical photolithography techniques followed by e-beam metal deposition of Ti/Au (10/150 nm) (see Supporting Information for detailed description). Rapid thermal annealing is then carried out in an ambient argon environment at a flow rate of 1000 sccm and a pressure of 3.62 Torr at the temperature of 200 to 500 °C for 1 min.

3. RESULTS AND DISCUSSION

Figure 1(a,c,d) illustrates the schematic of the devices under study for Transmission Line Method (TLM) and two terminal $I-V$ measurements using Keithley 4200 SCS system. For the measurements at high temperature, a semiautomated hot-chuck was used. The postfabrication annealing conditions on VO_2

thin-films is carried out by RTA in an ambient argon environment at a flow rate of 1000 sccm and a pressure of 3.62 Torr was applied at 200 °C, 300 °C, 400 °C, and 500 °C for 1 min. The effect of annealing conditions is first analyzed using TLM patterns. Figure 1b shows the TLM results where the total resistance is plotted with the length of the channel. As per conventional TLM theory, the slope of the curve gives the sheet resistance per unit width while the intersection on *y*-axis is the twice the contact resistance. As the curve between the total resistance vs length is a straight line, therefore, the nature of carrier transport at the ohmic contacts can be given by the transfer length concept as shown in the top-left inset of Figure 1c, where the carrier travels a certain length in the thin-film before entering the ohmic metal; this is to avoid the crowding effect at the junction. From the TLM theory, the relationship between the various resistances in the devices can be expressed as by the following expression:

$$R_T = 2R_C + (R_S/W)L \quad (1)$$

Using the above expression the sheet resistance and contact resistance are obtained for the annealed devices and plotted in Figure 1e. It can be seen from the figure that both resistances decrease with increase in the annealing temperature. The sheet resistance decreases from 375 kΩ/□ to 7.5 kΩ/□ for nonannealed device, mentioned as room-temperature sample (SRT), to devices annealed at 200, 300, 400, and 500 °C while the contact resistance also decreases from about 2 kΩ to almost zero for devices annealed at 400 and 500 °C. This fall in the sheet resistance can be attributed to the reducing effect which leads to oxygen deficiency in the thin-films. This deficiency has a doping effect in the VO_2 thin-films and results in higher concentration of electrons, thus higher conductivity and lower sheet resistance.

On the other hand, the fall in the contact resistance can be attributed to the better uniformity of the metal-thin-film interface and lower sheet resistance which results in better ohmic contacts. However, for the devices that are annealed beyond 300 °C, the measured contact resistance is almost zero, which may be due to the near metallic behavior shown by the annealed thin-films. TLM results sometimes gives erroneous small negative values around zero for such contact conditions as observed in Figure 1e.

In order to analyze the observed sheet resistance variations, X-ray photoelectron spectroscopy is carried out at room-temperature in vacuum. As vanadium is a transition element therefore annealing could have result in the change of the vanadium oxidation state which can be detected by the XPS analysis by comparing various parameters at V $2p_{3/2}$, V $2p_{1/2}$, and O 1s peaks such as peak shape and binding energy differences. Figure 2 shows the wide scan XPS spectra of the annealed devices. Different peaks are marked in the figure indicating that the levels near Fermi-level (0 V) have low binding energy while the inner levels, which are far away have higher binding energy.[14,15] It may be noted that the levels marked here are mostly the hybridized levels as per molecular orbital theory;[16] however, the orbital still maintains its strong behavior; therefore, the name of the level indicates the more prominent orbitals. In order to get the clear understanding of the energy levels involved in the VO_2 bonding, energy band diagram for both insulating and metallic states is shown in Figure 3. It can be seen that the outer 3d and 2p molecular orbitals of vanadium and oxygen, respectively, are involved in bonding as per the molecular orbital theory (V^{4+} = [He]-$2s^2 2p^6 3s^2 3p^6 3d^1$). As seen in the figure that the splitting of d_{11} orbital in the insulating state leads to localization of electrons and opening of an energy band gap. The resulting distortion on the lattice arrangement also leads to the minor correction in the energy level of Π* orbitals.[17]

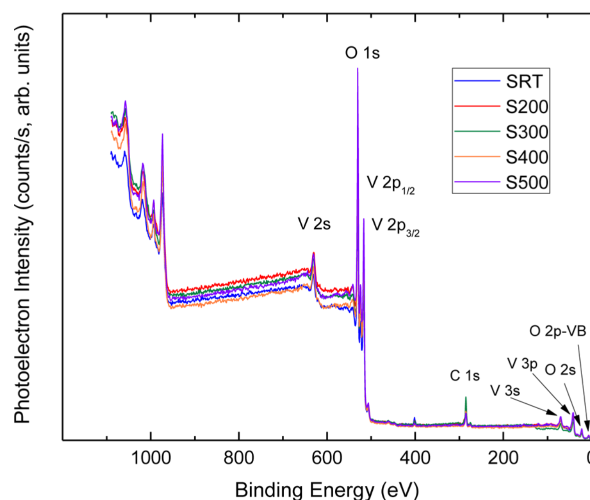

Figure 2. Wide scan XPS spectra in vacuum at room-temperature of the VO_2 thin-films annealed at various temperatures.

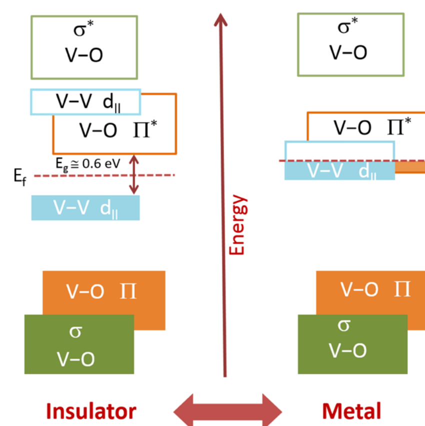

Figure 3. Schematic energy band diagram of the vanadium dioxide based on the molecular orbital theory illustrating the d_{11} band splits from metal to insulator transition. The symbol V−O and V−V stand for hybridized vanadium−oxygen and vanadium−vanadium orbitals, respectively.

Figure 4 plots O 1s and V 2p spectra with 2p doublet (V $2p_{3/2}$ and V $2p_{1/2}$) of all the devices. The red line denotes the fitted curve while the black line indicates the peak position using Lorentzian−Gaussian sum function. In XPS analysis, the binding energy and shapes of the peaks can be used as information to assess the chemical state and stoichiometry of the thin-film.[14] As can be seen from the figure that of all the peaks, the shape and position of mainly V $2p_{3/2}$ peak shows observable variations with annealing. The satellite peaks for both V 2p doublets are due to strong hybridization between V 3d and O 2p levels and are observed in various vanadium oxides including V_2O_5, VO_2, and V_2O_3. The V $2p_{3/2}$ peak in Figure 4 is composed of two peaks one at 516 eV and other at 517.2 eV which are related to the two oxidation state of V^{4+} and V^{5+}, respectively.[17−19] The observation of V^{5+} peaks in VO_2 thin-film surface is expected as the XPS is a surface characterization technique and VO_2 thin-film surface is prone to oxidation after

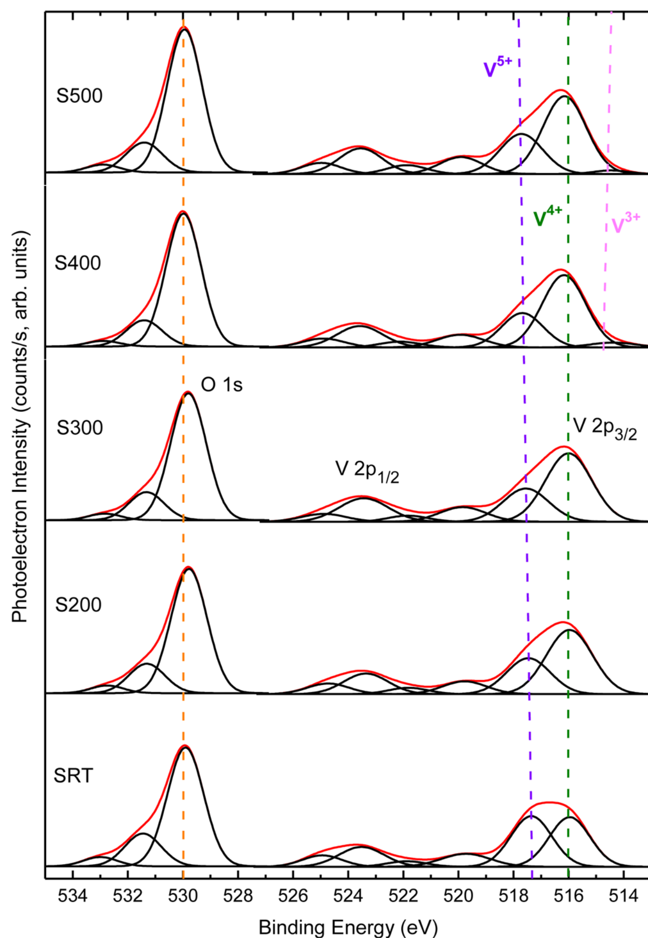

Figure 4. O 1s and V 2p XPS spectra in vacuum at room-temperature of the VO_2 thin-films annealed at various temperature. Orange, violet, green, and magenta lines indicate O 1s, V^{5+}, V^{4+}, and V^{3+} peaks in the spectra, respectively.

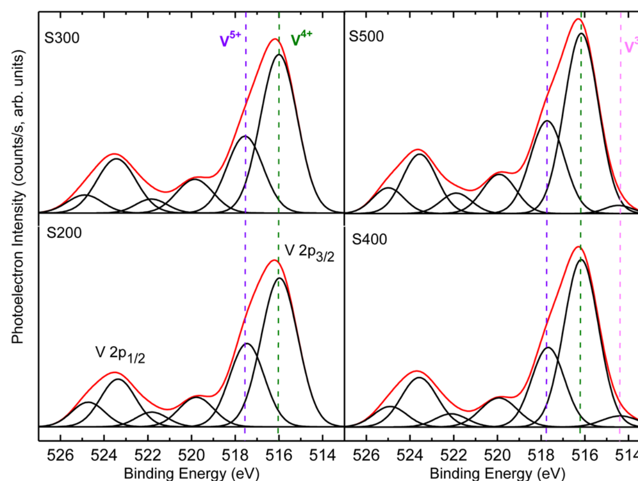

Figure 5. V2p doublet (V $2p_{3/2}$ and V $2p_{1/2}$) spectra in vacuum at room-temperature of the VO_2 thin-films annealed at various temperature. Violet, green, and magenta lines indicates V^{5+}, V^{4+}, and V^{3+} peaks in the spectra, respectively.

being exposed to atmosphere.[18] However, with annealing, the intensity of V^{5+} peaks decreases relative to the V^{4+} peak, which also confirms the reduction effects on the samples. The additional components with O1s peaks can be explained from the C1s peak observed in the full spectra of the samples in Figure 2, such satellite peaks at O1s has been attributed to C—O and C═O bonds, which can come from sample preparation or during processing steps.[17] The most notable feature is the evolution of a new peak at around 515 eV for samples annealed at 400 and 500 °C. This additional peak in the XPS spectra is related to the lower oxidation state of vanadium, most likely V^{3+} or other complex magneli phases. This reduction of vanadium implies the additional electron for $3d^2$ features, these extra electrons can also come from lattice defects and oxygen vacancies also. As a result of this, the transition temperature of the thin-films becomes lower than room-temperature and consequently the sheet−resistance decreases sharply as seen in Figure 1e. Figure 5 shows the zoom-in features of the V 2p doublet spectra in detail where the extra peak appearing in 400 and 500 °C annealed sample can be seen clearly. The evolution of peaks has also been analyzed using deconvolution method after subtracting the Shirley baseline,[12,20] where the variation in oxidation state with annealing can be seen (see Supporting Information). It may be noted that the dotted lines at the V $2p_{3/2}$ peaks in Figures 4 and 5 appears slightly outward; this is because, on reduction the relative position of V $2p_{3/2}$ and O 1s, peaks move away from each other due to higher binding energy of V^{3+} oxidation state.[20] Also, as the annealing process would result in gradation in composition due to diffusional constraints in the thin film, therefore, a depth dependent profile would have provide the required information regarding the steady state at a particular depth. However, in the absence of the depth profile in the present work due to function constraint, a similar result from Gopalakrishnan et al.[20] where the diffusion depth is reported to be around 30 nm under similar temperature conditions can be referred as the probable diffusion profile. Further, in order to analyze the impact of annealing temperature and time duration on the surface diffusion conditions and device characteristics, a time-dependent annealing at 200 and 300 °C has also been performed and would be discuss in the later sections.

With the characterization of sheet-resistance and spectra analysis, the transition property of the VO_2 thin-films is measured at various temperatures and the effect of annealing on the transition temperature is studied. In Figure 6a, voltage hysteresis curves are plotted for all the devices using a compliance of 10 mA to avoid excess current flow after the insulator−metal transition, which could burn the devices. Although various studies have focused on the mechanism and electrical and structural correlation of such transitions,[21,22] this work focus on the threshold-voltage (jump voltage) shift induced by annealing. As seen from the figure that the threshold voltage (V_{th1}), at which transition from insulating to metal phase occurs, is found to be decreasing with higher temperature annealed devices while the threshold voltage (V_{th2}), at which transition from metal to insulating phase occurs, is found to be almost invariant for all the devices. This variation in the threshold voltages can be explained on the basis of a simple power dissipation model. In this model, the power dissipation across the resistive thin-film can be expressed as follows.[23,24]

$$\frac{dQ}{dt} = \frac{V^2}{R} - k(T - T_o) \tag{2}$$

where k is a collection of thermal parameters, including the thermal coefficient and heat capacity of the thin-film and the underlying substrate, V and R are the voltage and resistance

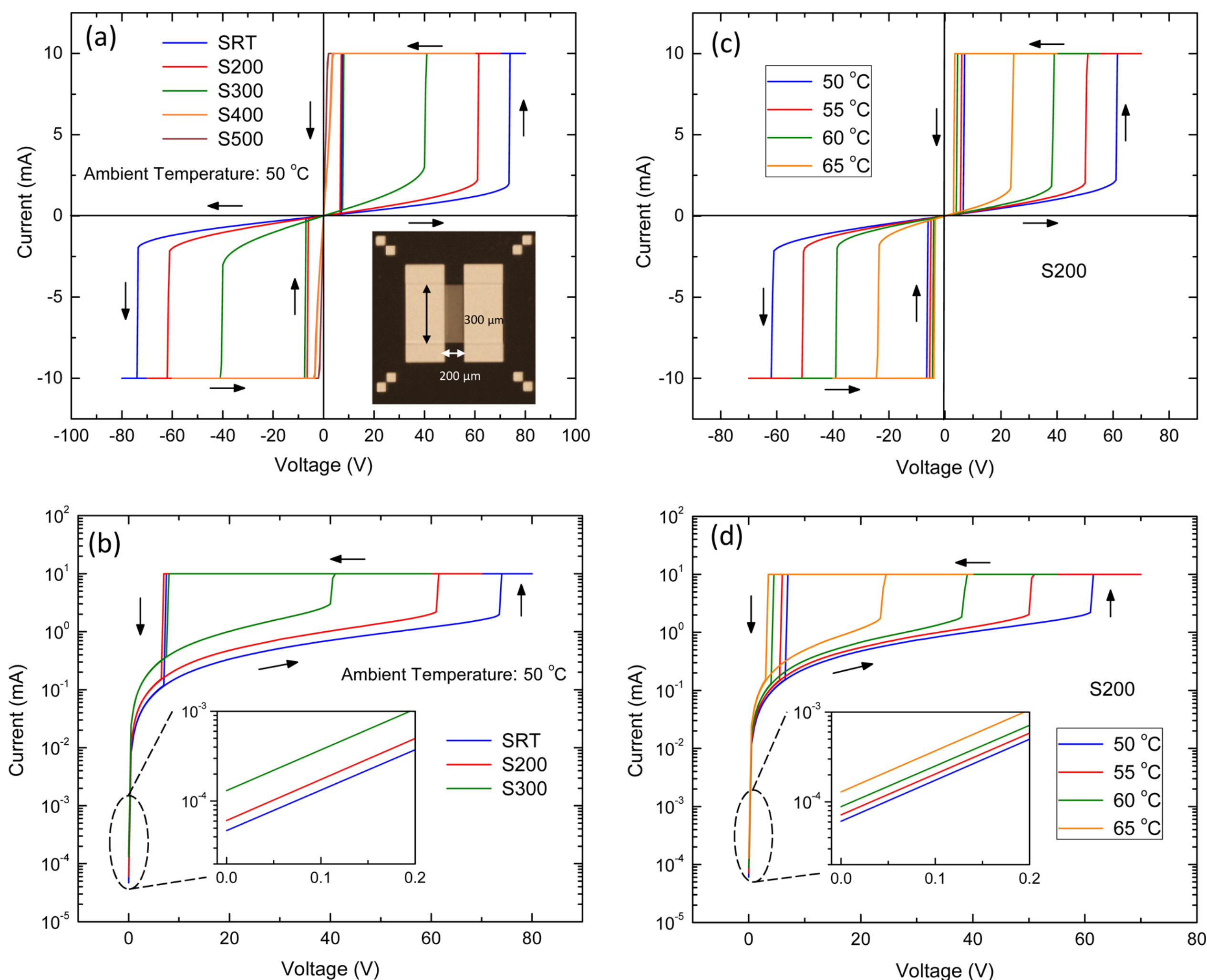

Figure 6. *I*−*V* curve of various devices at 50 °C ambient temperature with a compliance of 10 mA to avoid the excess current flowing through the samples. (a) Bidirectional dual-sweep *I*−*V* curve of various devices, the inset figure illustrates the fabricated device along with dimensions. (b) Semilogarithmic *I*−*V* plot of positive dual-sweep in a. (c) Bidirectional dual-sweep *I*−*V* curve of S200. (d) Semilogarithmic *I*−*V* plot of positive dual-sweep in c. Voltage sweep direction in a and c is from negative to positive direction and back to original value as indicated by arrows and the inset in b and d zoom-in the encircled data range for more clarity.

across the thin-film, respectively, and T and T_o are the temperature of thin-film and ambient environment, respectively. The power dissipation across the thin-film results in joule-heating which leads to a corresponding rise in the local temperature. The insulator−metal transition occurs when the rise in the local temperature due to joule-heating equals to the transition temperature of the thin-film. As the power-dissipation is counterbalanced by the conductive-losses thorough ambient environment, substrate, and metal electrodes, therefore, at equilibrium and negligible contact resistances, eq 2 can be simplified as follows:

$$V_{th1} = (k(T_C - T_o)R_A)^{1/2} \quad (3)$$

where R_A is the thin-film resistance before transition, V_{th1} and T_C are the threshold voltage and transition temperature, respectively. An analogous expression for V_{th2}, at which reverse transition occurs when voltage is swept from high to low values, can be similarly deduced:

$$V_{th2} = (k'(T_C - T_o)R_B)^{1/2} \quad (4)$$

where k' is the collection of thermal coefficients in the metallic phase at high temperature, and R_B is the NB resistance in the metallic phase.

It can be seen from eqs 3 and 4 that the thermal coefficient term is considered different because of the variation reported in the thermal conductivity of VO_2 thin-film across the transition point.[25−27]

According to eq 3, V_{th1} depends on several factors including thin-film resistance, thermal coefficient, and transition and ambient temperature as well. Thus, the observed variations in V_{th1} for similar ambient temperature and thermal coefficient terms can be explained by the decrease in the thin-film resistance by annealing treatment. The decrease in resistance results in the higher power dissipation on the account of joule-heating, thus reaching the threshold point earlier as compared to the higher resistive thin-films. Whereas, similar V_{th2} indicates that the resistance values of the thin-films in the metallic phase are almost constant and does not varies with the annealing temperature. Further, increase in threshold voltage with decreasing channel width is observed which also agree with eq 3 (see Supporting Information). Hysteresis obtained in voltage induced transition in VO_2 material is a characteristic

feature of the first order phase transitions, which is observed in temperature and photoinduced transitions as well. The transition from insulator to metal (metal to insulator) requires some amount of overheating (undercooling) above (below) the equilibrium transition temperature where the energy curves of the two phases intersect with a discontinuity in the first derivative, indicating a double-minima energy curve.[3,28] Besides hysteresis, characteristics such as variation in optical transmission properties across transition is also a characteristic feature of VO_2 thin-films (see Supporting Information).

In Figure 6b, it can be seen that with an increase in the leakage current near zero voltage (the residual current near zero voltage is termed as leakage current), the threshold voltage of the annealed devices decreases. This increase in off-current can be caused by the excitation of carriers in impurity levels such as oxygen deficiency, which varies with the annealing temperature of the devices. The correlation between the leakage current and the transition voltage can be explained by the hole-based theory of transition where a critical density of holes causes a breakdown of on-site Coulomb energy resulting in the transition.[21]

Figure 6c shows the variations in the threshold voltages of S200 with an increase in the ambient temperature. As seen from the figure, the threshold voltage decreases with the increase in the ambient temperature. This also agrees well with eq 3 as thermal activation at higher temperature results in lower resistance, which leads to higher joule-heating thus reaching the transition at lower voltages. Besides typical thermal activation across band gap, the decrease in resistance with temperature in VO_2 has also been linked to the coexistence of both electronic phases with a work-function difference of 0.18 eV.[29] In Figure 6d, the leakage current correlation with threshold voltage also agrees with the discussion for Figure 6b, with the difference that the increase in leakage current here is caused by the temperature activation.

In order to analyze the transition dynamics further, S200 curve for 50 °C is plotted in Figure 7 in terms of current density (J) and conductance (dI/dV) versus voltage (V) using the following expression $J = IA$ (A is the cross-sectional area) and dI/dV is the differential of the current curve with respect to voltage. At 61 V or 0.3 MV/m approx., an abrupt jump in dI/dV and J (point A1 and A2 in Figure 7) indicate a jump in conductivity which is closely related to the electron concentration ($J = \sigma E$ and $\sigma = ne\mu$). Although variations in mobility across transition have also been reported, they are less than an order, thus negligible, as compared to the variation in the carrier concentration. The abrupt jump in current density to the order of 10^4 A/cm^{-2} indicates the metallic behavior, although this value could go higher but limited by the current compliance at 10 mA. Initially, the dI/dV curve is independent of the applied voltage or electric field (line S1 in Figure 7); however, at higher voltage, it increases exponentially with increasing field (line S2 in Figure 7). The dI/dV at positive voltage is closely related to the density of states (DOS) above the Fermi level given by the relation;

$$\frac{dI}{dV} \approx \int_{-\infty}^{+\infty} N_F(eV)[-\partial f(E + eV, T)/\partial(eV)]dE \approx N_F(eV) \quad (5)$$

where $N_F(eV)$ is the DOS on the Fermi level and $f(E + eV,T)$ is the Fermi–Dirac function. As N_F (eV) is constant for metal, so the device can be regarded as a semiconductor below the transition point. This abrupt jump in dI/dV or DOS on Fermi surface indicates a first-order insulator metal transition as theoretically derived by Brinkman and Rice.[21] Further, the transition to metallic phase involves only Mott's transition; that is, the structure lattice remains intact in monoclinic. However, later on, it is followed by structural phase transition known as Peierls transition by an electron–phonon interaction.[21]

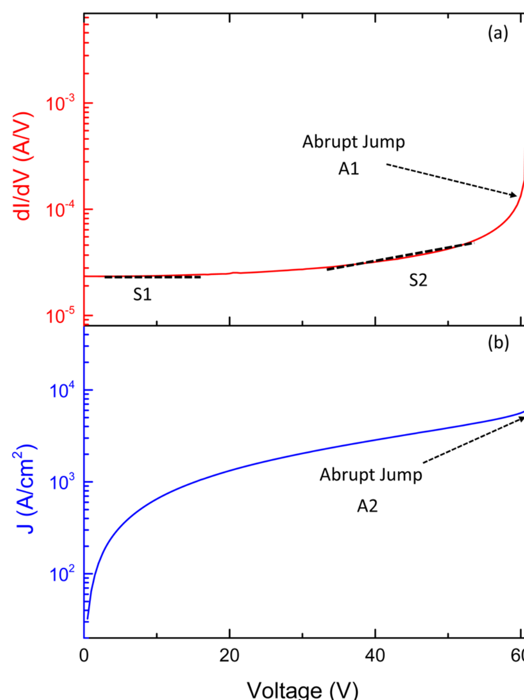

Figure 7. (a) Conductance (dI/dV) and (b) current density (J) versus voltage for S200 device at 50 °C is plotted in semilogarithmic scale. A1 and A2 indicate abrupt jump in conductance and current density, while lines S1 and S2 indicate the constant and exponential rise in dI/dV, respectively.

The observed lowering of threshold voltage in Figure 6 also fits the Mott's theory according to which the transition occurs at a critical density n_c, which measures the screening due to electron–electron interaction, given by[1]

$$(n_c)^{1/3}\alpha_H \cong 0.25 \quad (6)$$

where α_H is the localization radius of electrons in the insulating phase known as Bohr radius. As discussed above, both thermal activation and annealing result in increase in carrier concentration resulting in the lower threshold voltage. Therefore, an increase in carrier concentration at higher temperature requires lesser joule-heating to reach the critical carrier concentration resulting in lower threshold voltages.

In order to confirm the variation in the transition temperature with annealing, the square of eq 3 is plotted with ambient temperature in Figure 8a, where the intercept on x-axis gives the transition temperature for the respective device. As seen from the figure, T_C for SRT and S200 remain almost constant at 67.5 °C, but for S300, it recedes to 66 °C. These values matches within small error range to the thermal transition based values (see Supporting Information). This can be due to the various factors, which are not included in the power model such as strain, defects induced strain, etc., in particular, the higher density of oxygen deficiency-related defects in S300, which can act like electron donor and/or lattice deformers nucleation sites with lower free energy for first order

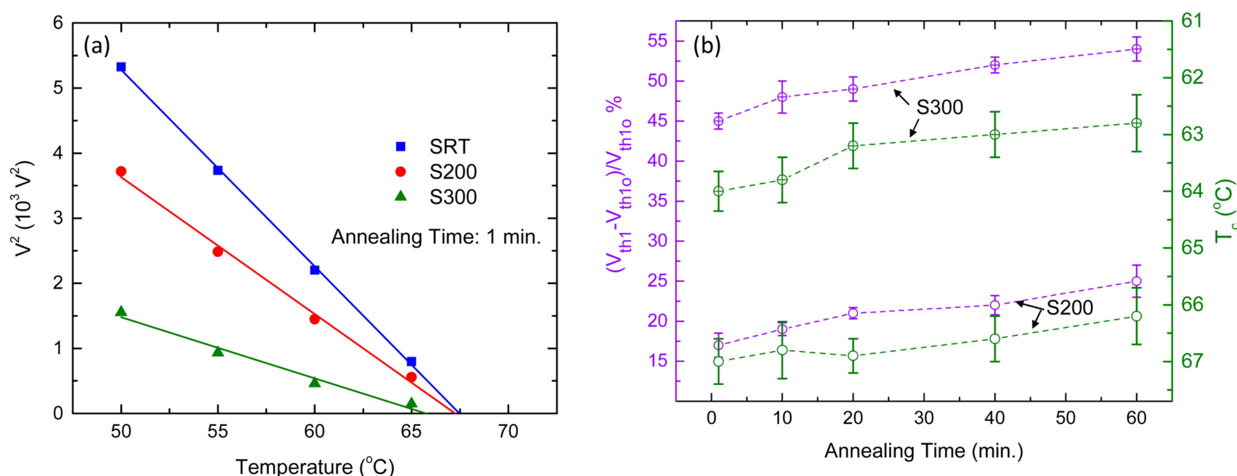

Figure 8. Variation in device characteristics with annealing temperature and time-duration (a) V^2 curve with temperature for SRT, S200, and S300 devices. The *x*-axis intercept gives the transition temperature. (b) Percentage variation in V_{th1} with annealing-time and transition temperature for S200 and S300 with annealing time varying from 1 to 60 min.

phase transition thus resulting in more difference between the theoretical and the measured T_C. The lowering of T_C can also be explained both from the critical holes and electron concentration based theories, where a critical density of carriers is required for transitions, as annealing results in higher conductivity, hence higher carrier concentration; therefore, a lesser temperature force is required to reach the critical density resulting in decrease in T_C. Similar decrease in T_C has been reported in other studies[30] where higher concentration was achieved by gold nanoparticles induced electron doping in the thin-film. Further, the lowering of device resistance due to annealing leads to variation in magnitude of current- and resistance-jump across the transitions. Besides, thermal measurement, metallic state resistance is measured using 1 kΩ external resistance in the *I*−*V* measurement (see Supporting Information), as seen from Figure 6a, where annealing results in lowering of resistance and transition point along with an increase in the threshold current. While, the threshold current increase from 1.86, 2.21, to 3.01 mA, but the resistance-jump decreases from 200, 134, and 55 for SRT, S200, and S300, respectively. As compared to the resistance variation in insulating state, resistance variation due to annealing is negligible in metallic state. This lowering of resistance and current-jump further validates the higher off-stoichiometry in annealed thin-film; however, the crystallinity of the thin-film is still maintained as evident from the well-shaped current and resistance jumps.[20] Further, in addition to 1 min duration annealing at different temperatures, annealing process has also been carried out for different time-duration, that is, 5, 10, 20, 40, 60 min at 200 and 300 °C, in order to see the effects of time-duration on the device characteristics. For each time−temperature combination, more than four devices of various dimensions has been tested and the variations obtained in both voltage and thermal induced annealing are plotted in Figure 8b. The variation in transition voltage is found to be dependent on both time and annealing temperature; however, it seems that temperature is a crucial factor, as it might determines the temperature dependent stability-threshold of vanadium in various oxidation states in the thin-film. Whereas, the time-dependence variation of transition voltage can be explained by the continuous diffusion process, which could results in further reduction, thus varying the device transition characteristics.

4. CONCLUSION

In conclusion, VO_2 thin-films were annealed at various temperature in reducing environment. Both chemical and electrical characterization were carried out for all the devices. XPS analysis confirmed oxygen deficiency, which resulted in reduced sheet resistance and slight decrease in transition temperature, as observed from the electrical/thermal measurements. The fall in the threshold voltage can be correlated with the decrease in the sheet resistance which in turn also reduces the transition temperature of the device. However, S400 and S500 showed almost metallic characteristics, which may be linked to the formation of V^{3+} states resulting in an increase in electron concentration exceeding the critical value thus stabilizing the metallic states even at the room-temperature. This study not only enriches the understanding of the complex phase transition process but also provides a method to tweak controllable properties for practical device applications.

■ ASSOCIATED CONTENT

Supporting Information

Raman spectra, device fabrication method, optical image of fabricated devices, both two-terminal and TLM pattern, AFM thickness measurement, *I*−*V* characteristic of devices with variable channel width. (Figures S1−S7) Schematic of device burn-out at high voltage and contrast image of the device channel after metal−insulator transition in the metallic state (Figure S8−S9) with various current compliance values (Figure S10). Deconvoluted peaks of V 2p3/2 for S200 and S500 device. (Figure S11) *R*−*T* curve, random fluctuation in *I*−*V* curve with 21 continuous sweep, and the curve to measure metallic resistance using external resistance. (Figure S12−S14) The burn-out and color change process during metal insulator transitions has also been captured and shown in the video clips. This material is available free of charge via the Internet at http://pubs.acs.org.

■ AUTHOR INFORMATION

Corresponding Author

*E-mail: ghkim@skku.edu.

Notes

The authors declare no competing financial interest.

ACKNOWLEDGMENTS

This research was supported by Basic Science Research Program through the National Research Foundation of Korea (NRF) funded by the Ministry of Education, Science and Technology (2013R1A2A2A01069023) and the creative project in ETRI.

REFERENCES

(1) Yang, Z.; Ko, C.; Ramanathan, S. Oxide Electronics Utilizing Ultrafast Metal−Insulator Transitions. *Annu. Rev. Mater. Res.* **2011**, *41*, 337−367.
(2) Imada, M.; Fujimori, A.; Tokura, Y. Metal-Insulator Transitions. *Rev. Mod. Phys.* **1998**, *70*, 1039−1263.
(3) Nakano, M.; Shibuya, K.; Okuyama, D.; Hatano, T.; Ono, S.; Kawasaki, M.; Iwasa, Y.; Tokura, Y. Collective Bulk Carrier Delocalization Driven by Electrostatic Surface Charge Accumulation. *Nature* **2012**, *487*, 459−462.
(4) Cocker, T. L.; Titova, L. V.; Fourmaux, S.; Holloway, G.; Bandulet, H.-C.; Brassard, D.; Kieffer, J.-C.; Khakani, M. A. E.; Hegmann, F. A. Phase Diagram of the Ultrafast Photoinduced Insulator−Metal Transition in Vanadium Dioxide. *Phys. Rev. B* **2012**, *85*, 155120.
(5) Eyert, V. VO_2: A Novel View from Band Theory. *Phys. Rev. Lett.* **2011**, *107*, 016401.
(6) Baik, J. M.; Kim, M. H.; Larson, C.; Yavuz, C. T.; Stucky, G. D.; Wodtke, A. M.; Moskovits, M. Pd-Sensitized Single Vanadium Oxide Nanowires: Highly Responsive Hydrogen Sensing Based on the Metal−Insulator Transition. *Nano Lett.* **2009**, *9*, 3980−3984.
(7) Strelcov, E.; Lilach, Y.; Kolmakov, A. Gas Sensor Based on Metal−Insulator Transition in VO_2 Nanowire Thermistor. *Nano Lett.* **2009**, *9*, 2322−2326.
(8) Sengupta, S.; Wang, K.; Liu, K.; Bhat, A. K.; Dhara, S.; Wu, J.; Deshmukh, M. M. Field-Effect Modulation of Conductance in VO_2 Nanobeam Transistors with HfO_2 as the Gate Dielectric. *Appl. Phys. Lett.* **2011**, *99*, 062114.
(9) Kim, H.; Kim, Y.; Kim, K. S.; Jeong, H. Y.; Jang, A.-R.; Han, S. H.; Yoon, D. H.; Suh, K. S.; Shin, H. S.; Kim, T. Y.; Yang, W. S. Flexible Thermochromic Window Based on Hybridized VO_2/Graphene. *ACS Nano* **2013**, *7*, 5769−5776.
(10) Zimmers, A.; Aigouy, L.; Mortier, M.; Sharoni, A.; Wang, S.; West, K. G.; Ramirez, J. G.; Schuller, I. K. Role of Thermal Heating on the Voltage Induced Insulator−Metal Transition in VO_2. *Phys. Rev. Lett.* **2013**, *110*, 056601.
(11) Ko, C.; Ramanathan, S. Observation of Electric Field-Assisted Phase Transition in Thin Film Vanadium Oxide in a Metal-Oxide-Semiconductor Device Geometry. *Appl. Phys. Lett.* **2008**, *93*, 252101.
(12) Ruzmetov, D.; Senanayake, S. D.; Narayanamurti, V.; Ramanathan, S. Correlation between Metal−Insulator Transition Characteristics and Electronic Structure Changes in Vanadium Oxide Thin Films. *Phys. Rev. B* **2008**, *77*, 195442.
(13) Kittiwatanakul, S.; Laverock, J.; Newby, D., Jr.; Smith, K. E.; Wolf, S. A.; Lu, J. Transport Behavior and Electronic Structure of Phase Pure VO_2 Thin Films Grown on c-Plane Sapphire under Different O_2 Partial Pressure. *J. Appl. Phys.* **2013**, *114*, 053703.
(14) Silversmit, G.; Depla, D.; Poelman, H.; Marin, G. B.; Gryse, R. D. An XPS Study on the Surface Reduction of V_2O_5 (001) Induced by Ar+ Ion Bombardment. *Surf. Sci.* **2006**, *600*, 3512−3517.
(15) Silversmit, G.; Depla, D.; Poelman, H.; Marin, G. B.; Gryse, R. D. Determination of the V2p XPS Binding Energies for Different Vanadium Oxidation States (V5+ to V0+). *J. Electron Spectrosc. Relat. Phenom.* **2004**, *135*, 167−175.
(16) Goodenough, J. B. The Two Components of the Crystallographic Transition in VO_2. *J. Solid State Chem.* **1971**, *3*, 490−500.
(17) Mrowiecka, J. S.; Maurice, V.; Zanna, S.; Klein, L.; Marcus, P. XPS Study of Li Ion Intercalation in V_2O_5 Thin Films Prepared by Thermal Oxidation of Vanadium Metal. *Electrochim. Acta* **2007**, *52*, 5644−5653.
(18) Mendialdua, J.; Casanova, R.; Barbaux, Y. XPS Studies of V_2O_5, V_6O_{13}, VO_2, and V_2O_3. *J. Electron Spectrosc. Relat. Phenom.* **1995**, *71*, 249−261.
(19) Demetera, M.; Neumanna, M.; Reichelt, W. Mixed-Valence Vanadium Oxides Studied by XPS. *Surf. Sci.* **2000**, *454*−*456*, 41−44.
(20) Gopalakrishnan, G.; Ramanathan, S. Compositional and Metal−Insulator Transition Characteristics of Sputtered Vanadium Oxide Thin Films on Yttria-Stabilized Zirconia. *J. Mater. Sci.* **2011**, *46*, 5768−577.
(21) Kim, H.-T.; Chae, B.-G.; Youn, D.-H.; Maeng, S.-L.; Kim, G.; Kang, K.-Y.; Lim, Y.-S. Mechanism and Observation of Mott Transition in VO_2-Based Two- and Three-Terminal Devices. *New J. Phys.* **2004**, *6*, 52.
(22) Kim, B.-J.; Lee, Y. W.; Choi, S.; Lim, J.-W.; Yun, S. J.; Kim, H.-T.; Shin, T.-J.; Yun, H.-S. Micrometer X-ray Diffraction Study of VO_2 Films: Separation between Metal-Insulator Transition and Structural Phase Transition. *Phys. Rev. B* **2008**, *77*, 235401.
(23) Baik, J. M.; Kim, M. H.; Larson, C.; Wodtke, A. M.; Moskovits, M. Nanostructure-Dependent Metal−Insulator Transitions in Vanadium-Oxide Nanowires. *J. Phys. Chem. C* **2008**, *112*, 13328−13331.
(24) Rathi, S.; Park, J. H.; Lee, I. Y.; Kim, M. J.; Baik, J. M.; Kim, G.-H. Correlation between Thermal Annealing Temperature and Joule-Heating based Insulator−Metal Transition in VO_2 Nanobeams. *Appl. Phys. Lett.* **2013**, *103*, 203114.
(25) Oh, D. W.; Ko, C.; Ramanathan, S.; Cahill, D. G. Thermal Conductivity and Dynamic Heat Capacity Across the Metal−Insulator Transition in Thin Film VO_2. *Appl. Phys. Lett.* **2010**, *96*, 151906.
(26) Maurer, D.; Leue, A.; Heichele, R.; Muller, V. Elastic Behavior Near the Metal−Insulator Transition of VO_2. *Phys. Rev. B* **1999**, *60*, 13249.
(27) Chen, J. K.; Liu, X. L.; Yaun, X.; Zhang, Y. L.; Gao, Y. F.; Zhou, Y. F.; Liu, R. H.; Chen, L. D.; Chen, N. F. Investigation of the Thermal Conductivities Across Metal−Insulator Transition in Polycrystalline VO_2. *Chin. Sci. Bull.* **2012**, *57*, 3393−3396.
(28) Stoliar, P.; Cario, L.; Janod, E.; Corraze, B.; Deudon, C. G.; Bourmand, S. S.; Guiot, V.; Tranchant, J.; Rozenberg, M. Universal Electric-Field-Driven Resistive Transition in Narrow-Gap Mott Insulators. *Adv. Mater.* **2013**, *25*, 3222.
(29) Sohn, A.; Kim, H.; Kim, D.-W.; Ko, C.; Ramanathan, S.; Park, J.; Seo, G.; Kim, B.-J.; Shin, J.-H.; Kim, H.-T. Evolution of Local Work Function in Epitaxial VO_2 Thin Films Spanning the Metal−Insulator Transition. *Appl. Phys. Lett.* **2012**, *101*, 191605.
(30) Xu, G.; Huang, C. M.; Tazawa, M.; Jin, P.; Chen, D.-M.; Miao, L. Electron Injection Assisted Phase Transition in a Nano-Au-VO_2 Junction. *Appl. Phys. Lett.* **2008**, *93*, 061911.